

PUBLISHED VERSION

Alfonso Chinnici, Graham J. Nathan, and Bassam B. Dally

Performance characteristics of a hybrid solar receiver combustor utilising hydrogen or syngas

AIP Conference Proceedings, 2019 / Richter, C. (ed./s), vol.2126, pp.090004-1-090004-8

© 2019 Author(s).

Originally published at: <http://dx.doi.org/10.1063/1.5117606>

PERMISSIONS

<https://aip.scitation.org/apc/authors/preppapers> **Preparing your manuscript**

<https://aip.scitation.org/pb-assets/files/publications/apc/8x11WordTemplates-1485291154537.zip>

LICENSE TO PUBLISH AGREEMENT FOR CONFERENCE PROCEEDINGS

Copyright License Checklist

Author Rights and Permitted Uses

Subject to the rights herein granted to AIP Publishing, each Copyright Owner retains ownership of copyright and all other proprietary rights such as patent rights in the Work.

Each Copyright Owner retains the following nonexclusive rights to use the Work, without obtaining permission from AIP Publishing, in keeping with professional publication ethics and provided clear credit is given to its first publication in an AIP Publishing proceeding. Any reuse must include a full credit line acknowledging AIP Publishing's publication and a link to the Version of Record (VOR) on AIP Publishing's site.

Each Copyright Owner may:

....

11. Deposit the VOR in an institutional or funder-designated repository 12 months after publication by AIP Publishing.

...

10 September 2020

Performance Characteristics of a Hybrid Solar Receiver Combustor Utilising Hydrogen or Syngas

Alfonso Chinnici^{1, a)}, Graham J. Nathan² and Bassam B. Dally²

¹*PhD, Research Fellow, School of Mechanical Engineering, Centre for Energy Technology, The University of Adelaide, SA 5005, Australia,*

²*School of Mechanical Engineering, Centre for Energy Technology, The University of Adelaide, SA 5005, Australia*

^{a)}Corresponding author: alfonso.chinnici@adelaide.edu.au

Abstract. The use of hybrid solar thermal devices, which harness the energy from both concentrated solar radiation and combustion, is receiving growing attention due to their potential to provide a firm and dispatchable thermal energy supply while lowering the costs of energy systems and assisting the penetration of renewable energy. The Hybrid Solar Receiver Combustor (HSRC), which directly integrates the function of a solar receiver and a combustor into a single device, is a particularly promising hybrid technology. Its design allows the receiver to operate in three modes: solar-only, combustion-only and a mixed-mode (a combination of both solar and combustion). Compared with the present state-of-the-art in hybrid solar-combustion systems (which collect the thermal energy from the solar and combustion sources in separate devices and then combine them subsequently), the HSRC offers a reduction in total infrastructure (and hence capital costs), heat-exchange surface area, start-up/shut-down losses and pollutant emissions, due to a reduced need to start-up the back-up combustion plant. Also, the use of the HSRC with renewable fuels (e.g. hydrogen, syngas) offers the additional potential for low-cost carbon neutral or carbon-negative energy, although no data on performance for systems fed with alternative fuels are presently available. To this aim, the present work provides the first direct measurement of the performance of a Hybrid Solar Receiver Combustor (HSRC) fed with hydrogen-based fuels. A laboratory-scale HSRC prototype operated in the Moderate or Intense Low oxygen Dilution (MILD) combustion regime was tested at a nominal capacity of 12-kW_{th} for both the combustion-only and mixed mode, using hydrogen and syngas (H₂/CO = 2/1 v/v) as fuels. A 5-kW_{el} xenon-arc lamp was used to simulate solar radiation into the device. The influence of the mode of operation on the thermal efficiency, heat losses, heat flux distribution within the cavity and pollutant emissions are reported for a range of values of the heat extraction. It was found that the combustion process can be successfully stabilised within the HSRC over a wide range of operating conditions, and in the mixed-mode of operation, providing ultra-low NO_x emissions. The thermal performance was found to be similar for all the modes of operation, despite the different nature of the two energy sources and fuel composition. Overall, this study highlights that, if renewable H₂ or syngas are used as fuels, the device can efficiently operate in all the modes of operation employing 100% renewable energy.

INTRODUCTION

The development of technologies to hybridise concentrating solar thermal energy and combustion technologies, is driven by the potential to provide both cost-effective CO₂ mitigation and firm supply¹⁻⁵. Such hybrid systems offer the potential to lower the costs of renewable energy while providing a firm and dispatchable source of heat/power by reducing the total infrastructure and by thermodynamic synergies^{3,6}, and by reducing the need for, or cost of thermal energy storage⁶. In addition, in the near term, hybrids between solar and combustion systems offer potential to lower the use of fossil fuels, while in the longer term they offer potential for carbon neutral or carbon-negative energy with relatively low cost if alternative, renewable fuels (e.g. hydrogen, biomass) are employed⁶. However, the majority of hybrid technologies reported to date utilise a solar receiver designed solely to harvest the solar energy and a combustor designed solely to harvest the energy from the fuel (with the two devices designed to run either in series or parallel). This results in significant heat losses and inefficiency while increasing the capital costs of the combined system⁷.

These limitations can potentially be avoided by ‘direct hybrids’, which harness the solar and combustion processes within a single device⁶.

Of all the ‘direct hybrids’ proposed to date, the Hybrid Solar Receiver Combustor⁸ (HSRC) has received the most attention. Its design allows the system to operate in three modes: solar-only (when the intensity of concentrated solar radiation is above a useful threshold), combustion-only (in the absence of sufficient direct or stored solar energy) and a mixed-mode (a combination of both solar and combustion, to manage short and/or long-term variability of the solar source). The mixed mode also offers potential to mitigate against thermal shock (due to possible rapid variations in the intensity of solar flux) and increased harvesting of low solar energy flux in comparison with other hybrid systems^{9,10}. Recently, a particular arrangement of HSRC, which integrates the Moderate or Intense Low oxygen Dilution (MILD) combustion regime into the device has also been proposed to offer the potential for enhanced heat transfer, ultra-low pollutant emissions and fuel flexibility in comparison with standard combustion processes¹¹. Despite its many potential benefits⁷⁻¹¹, it has the disadvantage of a compromised receiver-combustor design to extract the heat efficiently from both a concentrated solar radiation (CSR) source and a combined radiation/convection source (combustion). Also, while the potential benefits of the device have been demonstrated by techno-economics analyses and recently by some experimental evidence¹²⁻¹⁹, only limited measurements of the performance of direct hybrids are presently available, with no data for systems fed with alternative, renewable fuels, so that a systematic investigation is needed to better evaluate the potential benefits with these fuels and assess the influence of the fuel composition on performance. This is critical, as the use of ‘direct hybrids’ with renewable fuels offers the additional potential for carbon-negative energy with relatively low-cost (while also increasing the amount of renewable in the system)⁶.

Therefore, the present paper aims to meet the aforementioned needs by providing direct measurement of the performance of a laboratory-scale HSRC fed with hydrogen and syngas (which can be produced renewably) and operated in the MILD regime.

METHODOLOGY

Experimental Arrangement and Operative Conditions

The laboratory-scale HSRC employed in this study is schematically shown in Figure 1. All the key details of the device have been described in a previous work¹², so that only its key features are reported here. The device features a receiver-combustor designed to extract the heat efficiently from either a radiation source (solar) or a combined radiation/convection source (combustion). The experimental rig features an insulated cavity with an aperture ($d_{ap} = 60$ mm) to let the simulated CSR into it. The internal length (L_i) and diameter (D_i) are 700-mm and 300-mm, respectively. The inner surface is a coiled heat exchanger, HX, carrying the heat transfer fluid, HTF (air), and consisting of four contiguous sections. This to enable measurements of the rate of heat transfer through each section while also maintaining control of the wall temperature. A layer of alumina (50-mm thick), which surrounds the HX, and a layer of ceramic material (100-mm thick) are used to mitigate losses. The outer shell (3-mm thick) is made from 316L stainless steel.

N-type thermocouples were used to monitor the inlet and outlet HTF temperatures, and the surface temperature of the inner (alumina) layer (with an acquisition rate of 2 sec). The device also features six auxiliary fuel and air injectors that are employed when the device is operated under MILD combustion regime. The annular burner configuration consists of six jets with an inclination angle (α) of 30°, supplying air ($d_{air} = 4$ mm) and fuel ($d_{fuel} = 2$ mm) for combustion-only and mixed operations. The cavity also features a conical outlet (made in stoneware clay) with an outlet diameter (d_{out}) of 40 mm, and a swirl burner to close the aperture and preheat the cavity during combustion-only operations.

Electronic mass flow controllers (ALICAT MCR-series, $\pm 0.2\%$ accuracy) were used to control the flow rates of HTF, combustion air and fuel. For combustion operations, hydrogen (H_2) and syngas ($H_2/CO = 2/1$ v/v) were used as fuels. The equivalence ratio, ϕ , and the thermal capacity, P_{in} , were fixed at 0.9 and 12 kW, respectively. For the combustion-only mode of operation under MILD regime, the swirl burner was used to preheat the cavity and the HSRC was switched to MILD by injecting fuel through the auxiliary nozzles when the average cavity temperature exceeded the auto-ignition temperature of the fuel. No air combustion preheating and/or heat recovering from the exhaust gas were considered here. The receiver was operated at atmospheric pressure for all the cases investigated.

For the mixed mode, a 5-kWel short-arc xenon lamp²⁰ was used as the energy source while the device was operated in MILD with the aperture open (i.e. no swirl burner). A diverging beam was employed in this study by positioning the focal point at ≈ 45 mm from the aperture plane¹². With this arrangement, the total simulated solar energy introduced

into the receiver, \dot{Q}_s , was ≈ 0.8 kW. This value is based on the measured heat flux profiles reported by others²⁰. The solar-to-fuel energy input ratio (S/F) was fixed at 6.7%, which corresponds to the lower threshold of useful flux in a solar day and to periods of partial cloud cover.

For all the modes of operation, the tilt angle was fixed to 0° (horizontal position) while the total HTF flow rate (\dot{Q}_{HTF}) was varied in the range 150-1000 standard litres per minute (*slpm*). A TESTO 350XL (portable) gas analyser and a R-type thermocouple were used to monitor continuously the composition and temperature of the exhaust stream. Details of the warm-up and steady-state time, together with the definition of steady-state conditions and accuracy of the gas analyser for each species can be found in a previous work¹². Time-averaged temperatures were measured and recorded under steady-state conditions. In the present study, steady-state conditions were assumed when the values of all the measured temperatures did not vary of up to 10°C in 0.5 hr. The warm-up time of the receiver to reach steady-state operation from a cold state was of about 3.5 h, and each test required additional 1.5 hr.

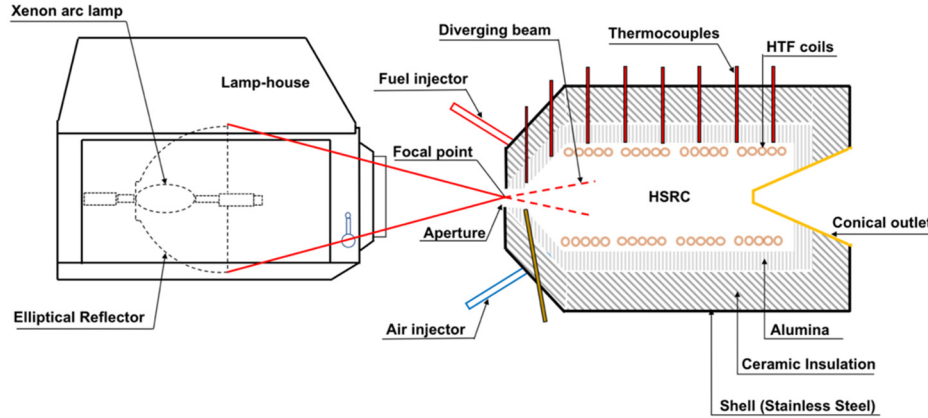


FIGURE 1. Schematic diagram of the experimental set-up, showing a side view of the laboratory-scale HSRC and the 5-kW_{el} short arc xenon lamp.

Heat Transfer Analysis

The heat transfer analysis employed in this work follows our previous works^{12,13}, so that only its key details are reported here. The overall energy balance can be described as follows:

$$\dot{Q}_f + \dot{Q}_a + \dot{Q}_s = \dot{Q}_{abs} + \dot{Q}_{ex} + \dot{Q}_{cond} + \dot{Q}_{rad} + \dot{Q}_{conv}, \quad (1)$$

where \dot{Q}_a and \dot{Q}_f ($\dot{Q}_f = \dot{m}_{fuel} * LHV$) represent the thermal input from the combustion air and fuel stream, respectively, and \dot{Q}_{abs} is the rate of energy absorbed by the HTF ($\dot{Q}_{abs} = \dot{m}_{HTF} * \sum_{i=1}^4 \bar{c}_{p,i} (T_{HTF,i} - T_{HTF,in,i})$, where \dot{m}_{HTF} is the HTF flow rate through each section of the HX, and $T_{HTF,i}$ and $T_{HTF,in,i}$ are the inlet and outlet HTF temperatures from each section of the HX, respectively). The terms \dot{Q}_{ex} , \dot{Q}_{cond} , \dot{Q}_{rad} and \dot{Q}_{conv} are the sensible heat in the exhaust, the conductive heat losses through the wall, the radiative and convective heat losses, respectively. Details regarding the measurements and calculation of each term can be found in previous works^{12,13}.

For each mode of operation, the ratio of the heat absorbed by the coil over the total thermal input (represented only by \dot{Q}_f , as air preheating was not considered here) is termed ‘absorption efficiency’, η_{abs} , and was calculated as follows¹²:

$$\eta_{abs} = \frac{\dot{Q}_{abs}}{\dot{Q}_f + \dot{Q}_s}. \quad (2)$$

To account for the influence of the heat recovery from the exhaust on the overall performance, a ‘potential thermal efficiency’, η_{th} , was also defined as follows:

$$\eta_{th} = \frac{\dot{Q}_{abs} + \dot{Q}_{HR,ex}}{\dot{Q}_f + \dot{Q}_s}, \quad (3)$$

Here, $\dot{Q}_{HR,ex}$ represents the sensible heat from the exhaust, calculated by assuming a value of 0.8 for the effectiveness of the heat exchanger ($\dot{Q}_{HR,ex}/\dot{Q}_{ex}$), as per previous investigations^{9,10,12,13}.

RESULTS AND DISCUSSION

Figure 2 presents the measured distribution of surface temperature of the alumina lining, T_c , along the length of the receiver, the heat flux distribution on the HTF coils, Q , and the NO_x and CO emissions for both combustion-only and mixed operations, for a fixed HTF flow rate (150 *slpm*) and by varying the fuel composition. It can be seen that a uniform temperature and heat flux distribution, typical of the MILD regime¹¹, features all the cases investigated. Furthermore, it can be seen that under MILD conditions, ultra-low NO_x emissions (< 15 ppmv) were measured for all cases. For the mixed mode, Figure 2 shows that the addition of CSR to the combustion process does not change the shape of the heat flux and wall cavity temperature (T_c and Q increased up to ~10% in the mixed mode compared with the combustion-only mode), indicating that operations in mixed mode do not influence the key characteristics of the MILD combustion process (uniform temperature and heat flux, ultra-low pollutant emissions).

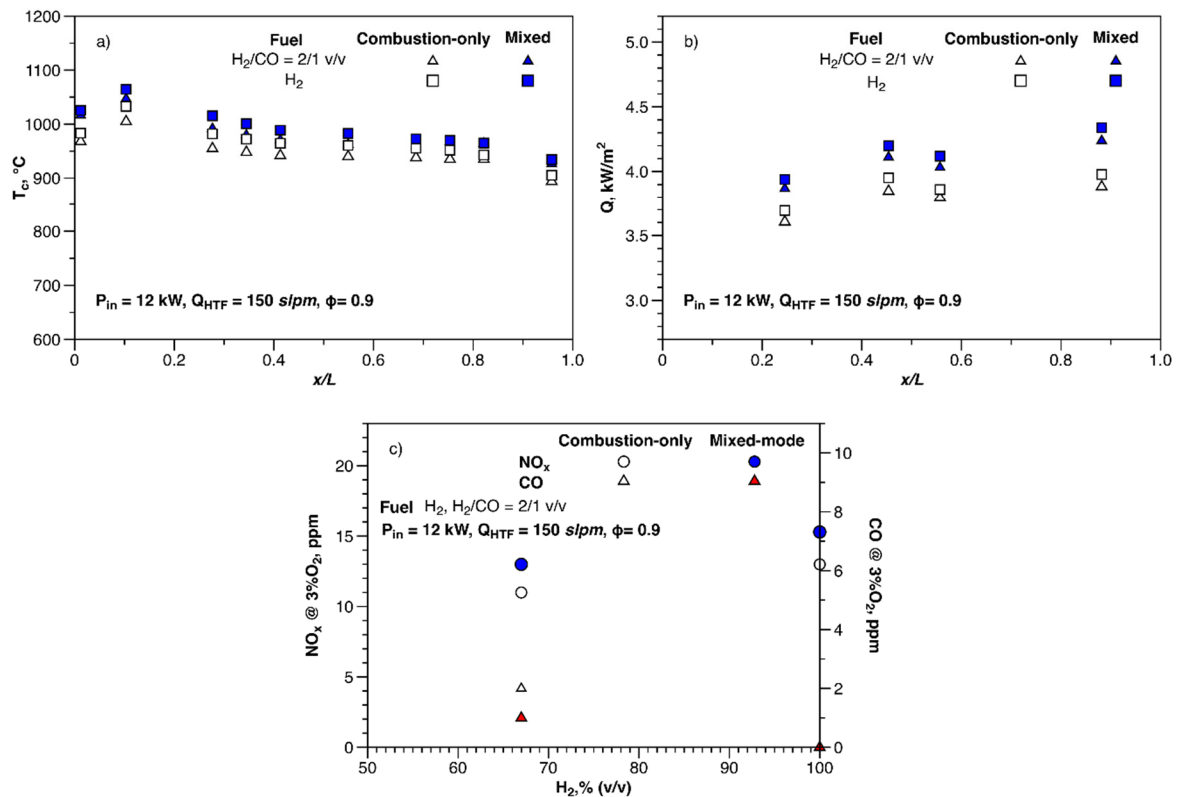


FIGURE 2. a) Axial distribution of the surface temperature of the alumina lining, T_c , b) heat flux through the HTF coils, Q , and c) NO_x and CO emissions for the combustion-only and mixed modes of operation, for a fixed HTF flow rate and by varying the fuel composition.

Figure 3 presents the values of the absorption (η_{abs}) and potential thermal (η_{th}) efficiencies, for combustion-only and mixed operations, and by varying the total HTF flow rate and fuel composition. The measured values of η_{th} for the solar-only mode^{12,13} are also reported. A comparison of η_{th} between combustion-only and mixed operations highlights that, regardless of the fuel composition, the device can achieve similar performance (of up to ~90%, assuming 80% of heat recovery from the exhaust) in both modes, with an outlet HTF temperature of up to ~800 °C. This provides evidence that the fuel flow rate can be used dynamically to compensate for variability in the solar resource. Furthermore, it can be seen that for all the range of Q_{HTF} , the measured values of η_{abs} for the mixed mode are higher than those for combustion-only operations (of up to ~15%, for a fixed value of Q_{HTF}). This indicates that, for

the operating conditions and geometry considered here, a net thermal gain can be obtained by adding CSR to the combustion process, notwithstanding the additional convective and re-radiation heat losses (<10%, see Table 1). In particular, despite a slight decrease in η_{th} (by $\sim 2.5\%$ in comparison with combustion-only operations) when operating the device in mixed-mode, the specific fuel consumption (sfc), i.e. the fuel consumption per unit of useful thermal output to the HTF, is significantly reduced (of up $\sim 20\%$, not shown) for mixed operations relative to the combustion-only case.

To further assess how the introduction of CSR influences the thermal performance of the device, Table 1 shows the values of heat losses for the two modes of operation and fuel composition investigated here, and for a fixed value of Q_{HTF} (150 $slpm$). The measured values of heat losses for the solar-only mode reported in previous works^{12,13} are also shown. For combustion operations and the different fuels considered, \dot{Q}_{ex} is the primary heat loss, as it accounts for $\sim 65\%$ of the total heat losses. Also, it is worth noting that the addition of CO to the H_2 stream leads to an increase in \dot{Q}_{ex} (despite a lower exhaust temperature, T_{ex}), as the sum of mass flow rates of fuel and combustion air required is greater (for a fixed P_{in} and ϕ). Also, the values of \dot{Q}_{rad} and \dot{Q}_{cond} for the H_2 case are higher than that of syngas case, due to a higher cavity temperature. For mixed operations, it can be seen that, despite the slight additional re-radiation and convective losses, an overall thermal benefit is achieved even by operating the device with a value of $S/F < 10\%$ (i.e. a relatively small amount of CSR is added to the combustion process). In particular, the contribution of \dot{Q}_{rad} and \dot{Q}_{conv} only account for 8 and 10% of the total heat losses, for syngas and H_2 cases, respectively. Also, it is worth noting that \dot{Q}_{conv} was minimal since the fraction of ambient air entrained into the device through the aperture was small (corresponding to $\sim 2-2.5\%$ of the inlet combustion air), for the different cases investigated. Similar trends were recently found for a HSRC fed with fossil fuels^{12,13}.

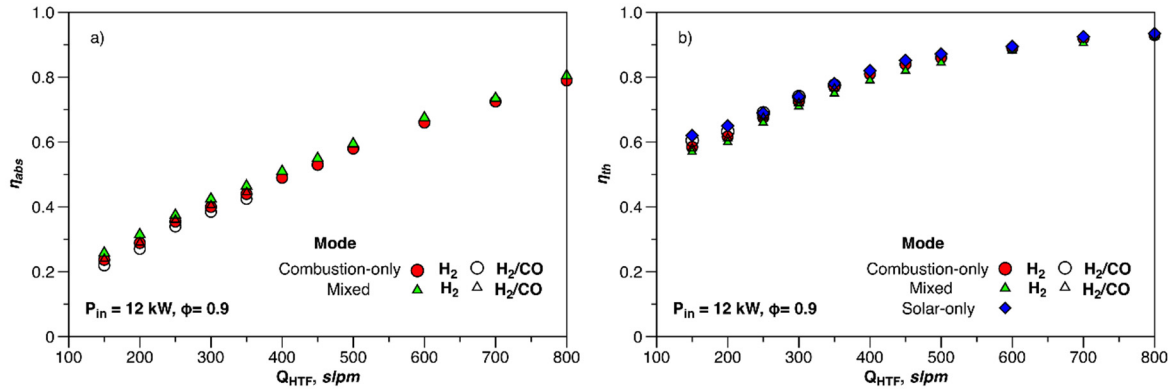


FIGURE 3. Values of a) absorption (η_{abs}) and b) potential thermal (η_{th}) efficiencies, for all the modes of operation, and by varying the total HTF flow rate and fuel composition.

TABLE 1. Values of heat losses (kW) for all the modes of operation ($Q_{HTF} = 150 slpm$).

Mode of operation	P_{in}, kW	Fuel	\dot{Q}_{ex}	\dot{Q}_{conv}	\dot{Q}_{rad}	\dot{Q}_{cond}
Combustion-only	12	H_2	4.8	/	0.28	3.75
Combustion-only	12	H_2/CO	5.45	/	0.19	3.3
Mixed-mode	12	H_2	4.62	0.29	0.62	3.8
Mixed-mode	12	H_2/CO	5.25	0.24	0.45	3.34
Solar-only ^{12,13}	0.8	/	/	0.18	0.003	0.12

CONCLUSIONS

The key outcomes from the experimental investigation on the performance characteristics of a laboratory-scale HSRC utilising hydrogen or syngas and operated in the solar-only, combustion-only and mixed modes are as follows:

- Successful, stable operations of a direct hybrid between a solar cavity receiver and a combustor have been reported for a wide range of operating conditions and fuel type for the three different modes;

- Similar thermal performance, in terms of heat flux, efficiency (up to ~90%) and emissions ($\text{NO}_x < 15$ ppm), can be achieved in the different modes, despite the different nature of the energy sources and their different heat transfer mechanisms. This provides confidence that reliable operation can be achieved when switching modes and/or fuel composition. Overall, this indicates that if renewable hydrogen or syngas are used as fuels, the device can operate efficiently in the three different modes of operation employing 100% renewable energy with ultra-low emissions and with the potential for carbon-neutral or carbon negative energy (depending on the routes and/or feedstock used to generate hydrogen or syngas).

ACKNOWLEDGMENTS

The authors gratefully acknowledge the support of the Australian Research Council and FCT Combustion and Vast Solar through the ARC Linkage Grant LP110200060.

REFERENCES

1. Moore, J., Apt, J., 2013. "Can hybrid solar-fossil power plants mitigate CO₂ at lower cost than PV or CSP?" in *Environmental Science Technology* **47** (6), 2487–2493.
2. Kolb, G.J., 1998. "Economic evaluation of solar-only and hybrid power towers using molten-salt technology," in *Solar Energy* **62** (1), 51–61.
3. Nathan, G.J., et al., 2017. "Research challenges in combustion and gasification arising from emerging technologies employing directly irradiated concentrating solar thermal radiation," in *Proceedings of the Combustion Institute* **36** (2), 2055–2074.
4. Kreith, F., Goswami, D.Y., 2007. Handbook of Energy Management and End Use Efficiency. CRC Press.
5. Peterseim, J.H., et al., 2013. "Concentrated solar power hybrid plants, which technologies are best suited for hybridisation?" in *Renewable Energy* **57**, 520–532.
6. Nathan, G.J., et al., 2018. "Solar thermal hybrids for combustion power plant: A growing opportunity," in *Progress in Energy and Combustion Science* **64**, 4–28.
7. Nathan, G.J., et al., 2014. "Economic evaluation of a novel fuel-saver hybrid combining a solar receiver with a combustor for a solar power tower," in *Applied Energy* **113**, 1235–1243.
8. Nathan, G.J., et al., 2013. "A hybrid receiver-combustor". US Patent 2015/0054284 A.R.I.P. Ltd.
9. Lim, J.H., et al., 2016. "Analytical assessment of a novel hybrid solar tubular receiver and combustor," in *Applied Energy* **162**, 298–307.
10. Lim, J.H., et al., 2016. "Impact of start-up and shut-down losses on the economic benefit of an integrated hybrid solar cavity receiver and combustor," in *Applied Energy* **164**, 10–20.
11. Lim, J.H., et al., 2016. "Assessment of the potential benefits and constraints of a hybrid solar receiver and combustor operated in the MILD combustion regime," in *Energy* **116**, 735–745.
12. Chinnici, A., et al., 2018. "Experimental demonstration of the hybrid solar receiver combustor," in *Applied Energy* **224**, 426–437.
13. Chinnici, A., et al., 2018. "An experimental study of the stability and performance characteristics of a Hybrid Solar Receiver Combustor operated in the MILD regime," in *Proceedings of the Combustion Institute*, in press, <https://doi.org/10.1016/j.proci.2018.05.099>
14. Lim, J.H., et al., 2016. "Techno-economic assessment of a hybrid solar receiver and combustor", in *AIP Conference Proceedings* **1734**, 070020.
15. Lim, J.H., et al., 2017. "Techno-economic evaluation of modular hybrid concentrating solar power systems," in *Energy* **129**, 158–170.
16. Lim, J.H., et al., 2017. "Assessing the techno-economics of modular hybrid solar thermal systems", in *AIP Conference Proceedings* **1850**, 110007.
17. Chinnici, A., et al., 2016. "Comparison of system performance in a hybrid solar receiver combustor operating with MILD and conventional combustion. Part I: Solar-only and combustion- only employing conventional combustion," in *Solar Energy* **147**, 489–503.
18. Chinnici, A., et al., 2016. "Comparison of system performance in a hybrid solar receiver combustor operating with MILD and conventional combustion. Part II: Effect of the combustion mode," in *Solar Energy* **147**, 479–488.

19. Chinnici, A., et al., 2018. "Thermal performance analysis of a syngas-fueled hybrid solar receiver combustor operated in the MILD combustion regime," in *Combustion Science Technology*, in press, <https://doi.org/10.1080/00102202.2018.1452381>
20. Dong, X., et al., 2015. "Concentric multilayer model of the arc in high intensity discharge lamps for solar simulators with experimental validation," in *Solar Energy* **122**, 293-306.